Metamorphic evolution of non-equilibrated granulitized eclogite from Punta de li Tulchi (Variscan Sardinia) determined through texturally controlled thermodynamic modelling

UNIVERSITÀ DEGLI STUDI DI TORINO

Journal of METAMORPHIC GEOLOGY

Texturally and compositionally non-equilibrated granulitized eclogite from Punta de Li Tulchi, Sardinian Variscan chain: a microstructural and thermodynamic study

Journal:	*Journal of Metamorphic Geology*
Manuscript ID:	JMG-11-0076.R2
Manuscript Type:	Original Article
Date Submitted by the Author:	09-May-2012
Complete List of Authors:	Cruciani, Gabriele; Università degli Studi di Cagliari, Dipartimento di Scienze Chimiche e Geologiche Franceschelli, Marcello; Università degli Studi di Cagliari, Dipartimento di Scienze Chimiche e Geologiche Groppo, Chiara; Università degli Studi di Torino, Dipartimento di Scienze della Terra Spano, Elena; Università degli Studi di Cagliari, Dipartimento di Scienze Chimiche e Geologiche
Keywords:	granulitized eclogite, corona textures, P-T pseudosection, Variscan Sardinia

Metamorphic evolution of non-equilibrated granulitized eclogite from Punta de li Tulchi (Variscan Sardinia) determined through texturally controlled thermodynamic modelling

G. CRUCIANI[1], M. FRANCESCHELLI[1*], C. GROPPO[2], M.E. SPANO[1]

[1] *Dipartimento di Scienze Chimiche e Geologiche, Via Trentino 51, Università degli Studi di Cagliari, I-09127, Cagliari, Italy*
[2] *Dipartimento di Scienze della Terra, Università degli Studi di Torino, via Valperga Caluso 35, 10125 Torino, Italy*

*Corresponding author: Marcello Franceschelli
Dipartimento di Scienze della Terra
Via Trentino, 51-09127 Cagliari, Italy
Tel. +39-070-6757713, Fax. +39-070-282236
E-mail: francmar@unica.it

ABSTRACT
The metamorphic evolution of a granulitized eclogite from Punta de li Tulchi NE Sardinia, Italy, reconstructed utilizing a combined microstructural (symplectitic, coronitic and kelyphytic features) and thermodynamic approach, involved a complex metamorphic history with equilibrium attained only at a domainal scale. Microstructural analysis and mineral zoning allow recognition of reactants and products involved in successive balanced mineral reactions. The *P-T* conditions at which each microstructure was formed are further constrained by calculating isochemical phase diagrams (pseudosections) for the composition of effectively reacting domains. A pre-symplectite stage developed during prograde metamorphism under conditions ranging from 660-680°C, 1.6-1.8 GPa to 660-700°C at 1.7-2.1 GPa. Pseudosections calculated for subsequent clinopyroxene + plagioclase and orthopyroxene + plagioclase symplectitic coronae using the composition of effectively reacting microdomains suggest temperature in excess of 800°C and pressures of 1.0-1.3 GPa. Modelling the development of later plagioclase + amphibole coronae around garnet during decompression yields conditions of 730-830°C and 0.8-1.1 GPa. H_2O (wt%) isomodes indicate that the granulitized eclogites were H_2O-undersaturated at peak-P conditions and during most of the subsequent heating and decompression. This allowed the preservation of prograde garnet zoning in spite of the strong granulite-facies overprint. The P-T evolution of Punta de li Tulchi granulitized eclogite is very similar in shape to that registered by other NE Sardinia retrogressed eclogites thus suggesting a common tectonic scenario for their evolution.

Key words: granulitized eclogite, corona textures, *P-T* pseudosection, Variscan Sardinia

INTRODUCTION

The European Variscan belt is well known for the widespread occurrence of rocks that experienced extreme metamorphic conditions, from the high/ultra-high pressure (HP/UHP) eclogite-facies conditions to high/ultra-high temperature (HT/UHT) granulite-facies conditions (e.g. Nasdala & Massonne, 2000, Massonne 2001; Lardeaux *et al*., 2001; Rötzler & Romer, 2001). The unusual high peak *P-T* conditions registered by these rocks suggest a tectonic scenario dominated by relatively high d*T*/d*P* gradients (e.g. O'Brien, 2008), in contrast with the low d*T*/d*P* gradients typical of mature subduction zones. Knowledge of the metamorphic evolution of these rocks is therefore highly relevant to orogenic processes. Several studies have estimated peak *P-T* conditions of eclogites and/or granulites in the European Variscan orogen (see O'Brien & Rötzler, 2003 for a review). However, petrological modelling of the complete *P-T*-(t) paths has only progressed in recent times. The majority of *P-T*-(t) paths for the European Variscan eclogites and/or granulites are based on *P-T* results of conventional thermobarometry, *P-T* grids and/or multi-equilibrium thermobarometry (PTGibbs and TWQ methods) (e.g. Bohemian Massif: O'Brien *et al*., 1997, Willner *et al*., 1997, Rötzler & Romer, 2001, Nakamura *et al*., 2004; Massif Central: Lardeaux *et al*., 2001, Berger *et al*., 2010; Argentera Massif: Ferrando *et al*., 2008; SE Corsica: Giacomini *et al*., 2008; NE Sardinia: Franceschelli *et al*., 1998, Cortesogno *et al*., 2004, Giacomini *et al*., 2005a). More recently, the pseudosection approach has been successfully applied to the study of the metamorphic evolution of Variscan granulites (e.g. Štípská *et al*., 2006; Tajčmanová *et al*., 2006; Racek *et al*., 2006; Cruciani *et al*., 2011).

Independent of the method used, reconstructing the *P-T*-(t) evolution of the European Variscan HP/HT rocks is particularly challenging because most are granulites derived from former eclogites. Consequently, original HP minerals usually show the effects of a HT overprint and are only locally preserved. For example, omphacite is commonly transformed into plagioclase +

clinopyroxene symplectites, and mineral compositions commonly re-equilibrated under high-temperature conditions. Symplectitic, coronitic and kelyphytic reaction textures are very common in these rocks and witness lack of textural equilibrium. Compositional equilibrium is at best attained at microdomainal scale. For example, plagioclase compositions may vary significantly between different reaction domains.

The success of the pseudosection method closely relies on the preliminary and detailed interpretation of the reaction textures (O'Brien & Ziemann, 2008; Powell & Holland, 2008) to identify the effectively reacting equilibration volume. This paper applies this approach to a granulitized eclogite from the Punta de li Tulchi outcrop in Variscan Sardinia. Franceschelli *et al*. (1998) already recognized the multi-stage *P-T* evolution of these rocks based on conventional thermobarometry and petrogenetic grids. However, the here presented new microstructural interpretation of reaction textures and corresponding pseudosections allows a considerable refinement of the metamorphic evolution (including the prograde segment) by solving the problem of domainal textural and compositional equilibrium.

GEOLOGICAL SETTING

The Sardinian Variscan chain consists of the following tectono-metamorphic zones with metamorphic grade increasing from SW to NE (Fig. 1): (i) the External Zone, (ii) the Nappe Zone, further subdivided into the External and Internal Nappe Zones, and (iii) the Internal or Axial Zone (Carmignani *et al*., 2001 and references therein). The Axial Zone is subdivided into a Migmatite Complex known as the High-Grade Metamorphic Complex (HGMC) and a southern Low to Medium-Grade Metamorphic Complex (L-MGMC) separated by the Posada-Asinara tectonic line (Fig. 1a,b). Metamorphic grade of metapelites and metapsammites in NE Sardinia rapidly increases towards the NE through a Barrovian sequence consisting of a biotite, garnet, staurolite + biotite, kyanite+biotite, sillimanite, and sillimanite + K-feldspar zone. The garnet zone is subdivided into garnet + albite and garnet + albite-oligoclase zones (Franceschelli *et al*., 2005).

In northern Sardinia five Variscan deformations have been recognized (Franceschelli *et al*., 2005; Helbing *et al*., 2006). The earliest of these (D_1) is witnessed by rare intrafoliar folds and relic S_1 cleavage (Elter *et al*., 1986), D_2 generated the most pervasive folds with E-W trending axes and an associated S_2 schistosity dipping S to SW. This phase has been interpreted in terms of transpressional tectonics by Carosi & Palmeri (2002). The D_3 phase produced open folds associated with a spaced crenulation cleavage but attaining the character of a pervasive schistosity (S_3) north of Olbia. In the fault rocks of the Posada Valley shear zone (Elter *et al*., 2010), a D_4 phase is recognized from shear bands and associated crenulation cleavages indicating a component of top to the NW followed by a top to the NE/SE shearing. In the same shear zone, D_5 produced a large flexure parallel to the orogenic trend, witnessed by the uplift of the Axial Zone with respect to the schistose envelope (Helbing *et al*., 2006).

Outcrops of metabasites preserving eclogite facies relicts only occur in the Axial Zone surrounded by migmatites and gneisses of the HGMC or within mylonitic schists and gneisses of the L-MGMC (Fig. 1a). Metabasites with eclogite-facies relicts are known since the pioneering work of Miller *et al*. (1976). More recent work has mainly concentrated on eclogitic rocks of the Migmatite Complex (Franceschelli *et al*., 1998., 2007; Cortesogno *et al*., 2004; Giacomini *et al*., 2005a) and of the L-MGMC (Cortesogno *et al*., 2004). Cortesogno *et al*. (2004) recognized different types of eclogites with different tectono-thermal evolution in the Migmatite Complex versus the L-MGMC. Franceschelli *et al*. (1998) and Giacomini *et al*. (2005a) recognized the polyphase metamorphic evolution of retrogressed eclogites from Punta de li Tulchi (Fig. 1c) and Golfo Aranci respectively. They distinguished five metamorphic stages corresponding to a pre-eclogite-, eclogite-, granulite-, amphibolite- and greenschist-facies conditions.

SHRIMP U-Pb dating of zircons of the Punta de li Tulchi retrogressed eclogites (Palmeri *et al*., 2004) yielded weighted means of 453 ± 14Ma, 400 ± 10Ma and 327 ± 7 Ma interpreted to represent the protolith age, the high- pressure eclogitic event (or Pb loss during the Variscan event), and amphibolite-facies retrogression, respectively. A similar protolith age (460 ± 5 Ma) was obtained by Giacomini *et al*. (2005a) from magmatic zircon preserved in the Golfo Aranci eclogites. These ages also agree with an age of 457 ± 2 Ma obtained by Cortesogno *et al*. (2004) for a first zircon population recovered from an eclogite body in the Migmatite Complex. A second zircon population yielded an age of 403 ± 4 Ma and was interpreted as the age of zircon crystallization during the high-grade event, probably the eclogite event. Zircon ages for eclogites of the Migmatite Complex cluster around the Early Visean (326-345Ma), interpreted as the age of the HP event, and between the Late Visean and Stephanian (304-299Ma), attributed to post-HP amphibolitic re-equilibration (Giacomini *et al*., 2005b). Based on correlations between the Maures Massif, Corsica-Sardinia Block, and Northern Apennine segments of the Variscan Belt, Elter & Pandeli (2005) propose a common structural-metamorphic evolution from the Early Carboniferous syn-collisional event to the Late Carboniferous-Early Permian, extensional shearing.

FIELD GEOLOGY

The Punta de li Tulchi retrogressed eclogite crops out as an E-W oriented, 100 m long × 20-30 m thick lens embedded within the nebulitic migmatites of Porto Ottiolu locality (Fig. 1c). The lens is parallel to the E-W-oriented pervasive regional schistosity of the hosting migmatites which also contain some decimeter-sized eclogite nodules near to the main eclogite body. Towards the south, the contact between the main eclogite body and the surrounding migmatite is marked by a meter-sized granitic body. The Punta de li Tulchi outcrop consists of a regular alternation of brownish garnet-pyroxene-rich and greenish amphibole-plagioclase-rich layers (Fig. 2a), striking E-W and dipping 50°N. The contact between these layers is sharp or transitional. Garnet-pyroxene-rich layers in turn exhibit an internal layering defined by alternating dark, garnet-rich, and white, clinopyroxene + plagioclase symplectite-rich, layers that are generally parallel to the S_2 in the surrounding migmatites. Locally, however, individual lobes of the symplectitic lamellae are oblique to S_2 (Fig. 2b,c), possibly indicating mimetic growth along a pre-existing S_1 schistosity. According to Franceschelli *et al*. (2007) an amphibole-rich front with vanishing boundaries clearly cuts the S_2 in the garnet-pyroxene layers. The amphibole + plagioclase-rich layers show an E-W oriented S_2 foliation followed by a N80-SE30°-oriented S_3 foliation, defined by the alignment of elongated millimeter-sized white pods (Fig. 2d). Locally, the S_3 foliation is crosscut by late shear zones (Fig. 2d), containing a mylonitic foliation with aligned coarse-grained biotite flakes.

The host migmatite is an orthogneiss containing a weak S_2 foliation oriented N 100° SW 45°. The age of the igneous protolith is unknown but a similar orthogneiss from Golfo Aranci and near Tanaunella yielded zircon ages of 469 ± 3.7Ma (Giacomini *et al*., 2006) and 458 ± 7 Ma (Helbing *&* Tiepolo, 2005), respectively. The orthogneiss consists of zoned microcline, Na-rich plagioclase, quartz, biotite, ± garnet, and late crosscutting muscovite. Towards Punta de li Tulchi, the biotite content of the migmatised orthogneiss decreases and the rocks acquire a nebulitic appearance. Leucosomes align parallel to the main S_2 foliation and also along the later shear zones. The migmatised orthogneiss is crosscutted by subvertical granitic dykes striking N 130° and ranging in thickness from a few meters to a several decameters.

PETROGRAPHY AND MICROSTRUCTURAL FEATURES

The studied granulitized eclogites contain variable amounts of garnet, omphacite, Ca-clinopyroxene, orthopyroxene, amphibole, plagioclase, biotite and quartz, with accessory epidote, rutile, ilmenite and apatite, monazite, zircon and very rare titanite, Fe-oxide and Fe-sulphides (Figs

3 & 4). The modal abundances of these minerals vary significantly for garnet-pyroxene versus amphibole-plagioclase rich layers described separately below.

Garnet + pyroxene layers

The garnet + pyroxene layers mainly consist of garnet, clinopyroxene, plagioclase and amphibole. Garnet forms anhedral, strongly fractured, poikiloblasts up to 5 mm in size (Fig. 3a) containing multiple omphacite inclusions (Cpx_1, mineral abbreviations according to Fettes & Desmons, 2007) up to 300-400 μm in length (Fig. 3b). Garnet also includes euhedral amphibole grains (Am_1) up to ~50-70 μm in size and quartz (Fig. 3c), as well as rounded grains of apatite. In both garnet and omphacite, several tiny rutile grains (Fig. 3b,c) and inclusions of zoned epidote grains (up to a few tens of microns in size) were found. Omphacite inclusions in garnet have a very thin and sharp, light colored rim of diopsidic clinopyroxene. Omphacite is rare in the matrix, but locally occurs as large crystals containing small quartz and Fe-sulphides inclusions. Omphacite in garnet is commonly partially replaced, mostly at the rim, by Cpx+Na-Pl symplectite.

The most striking feature of the retrogressed eclogites is the very fine grained intergrowths between clinopyroxene (Cpx_2) and plagioclase (Pl_1) lamellae (Cpx_2+Pl_1 symplectite, Fig. 3d-f), as also commonly observed in other metabasite lenses with eclogite-facies relicts from NE Sardinia (Franceschelli *et al*., 2007). The Cpx_2+Pl_1 symplectite is widespread in the matrix and replaces former omphacite, only locally preserved as very rare relicts. Although pyroxene in the symplectite is mostly clinopyroxene, in a few samples symplectitic orthopyroxene (Fig. 3e) is also present. Where both ortho- and clinopyroxene occur in the symplectite, they usually occur separately in two distinct symplectite types (i.e. Cpx_2+Pl_1 and Opx+Pl_1). However, where the two symplectites are in contact (Fig. 3e) and despite the sharp boundary between them, the orientation of the plagioclase lamellae does not vary significantly and some lamellae are continuous across this boundary (Fig. 3e). Orthopyroxene is generally found in two different microstructural positions: (i) as anhedral crystals associated with the Cpx_2+Pl_1 symplectite around garnet porphyroblasts, but not having themselves a symplectitic appearance (Fig. 3d,f) and, (ii) as a more or less continuous corona surrounding corroded quartz grains in the matrix (Fig. 4b). In both the cases, orthopyroxene is commonly partially replaced by cummingtonite (Am_2) at the outermost rim (Figs 3f & 4b).

Garnet porphyroblasts embedded within the Cpx_2+Pl_1 symplectite are in turn surrounded by well-developed composite corona microstructures (kelyphites, Figs 3a,b,d,e & 4a). The kelyphite consists of a continuous, thin plagioclase layer (Pl_2) associated with blebs of coronitic amphibole (Am_3) and anhedral ilmenite (Fig. 4a). The thickness of the Pl_2+Am_3 corona ranges between ~ 70 and 300 μm. Anhedral orthopyroxene and ilmenite crystals discontinuously occur at the outer margin of the Pl_2+Am_3 corona, in contact with the Cpx_2+Pl_1 symplectite. Both orthopyroxene and ilmenite are locally corroded by coronitic amphibole. Amphibole also occurs as brownish to pale-green, frequently zoned crystals (Am_4) in the rock matrix (Fig. 4c) and as minor late actinolitic amphibole (Am_5) growing at the expense of pyroxene or Am_4 in the rock matrix.

Biotite occurs (i) as very rare small inclusions in garnet, (ii) as small flakes aligned along S_2 and S_4 in the matrix or corroding garnet and amphibole crystals, and (iii) in the most re-equilibrated samples also as coarse-grained up to 0.5 mm sized crystals in several decimeter-thick shear zones.

Amphibole + plagioclase layers

The amphibole + plagioclase layers (Fig. 2a) are made up of "elongated white pods" (Franceschelli *et al*., 1998, Fig. 2d) mainly deriving from the intimate intergrowth of plagioclase with greenish and brownish amphibole (Fig. 4d) replacing garnet, relics of which are sometimes found in the cores of white pod. Other minerals identified in these layers are ilmenite, quartz, titanite, as well as rare biotite and chlorite. Amphibole is by far the most abundant mineral occupying up to 50-60 vol% and defining the S_2 foliation, whereas S_3 is defined by the shape elongation of the white pods.

MINERAL CHEMISTRY

The chemical composition of minerals from two garnet-pyroxene layer samples (E9, E10) and one amphibole-plagioclase layer sample (E19) was determined with a fully automated Cameca SX 50 electron microprobe at the IGAG-CNR Roma. Operating conditions were 15 kV accelerating voltage, a beam current of 15 nA and a 5–10 μm variable spot size. Natural and synthetic wollastonite, olivine, corundum, magnetite, rutile, orthoclase, jadeite, pure Mn, pure Cr, fluoro-phlogopite, and baryte were used as standards. Microstructural study, BSE imaging, and additional EDS analyses were performed with a FEI Quanta 200 SEM equipped with an EDAX-EDS detector at Cagliari University. Selected microprobe analyses of garnet, clino- and orthopyroxene, plagioclase, amphibole, and ilmenite of sample E9 are reported in Table 1, whereas those of samples E10 and E19 are reported in Tables S1, S2. Mineral compositions, including additional analyses not reported in Tables 1,S1,S2, are plotted in Figs 5, 6b, 7. Structural formulae have been calculated on the basis of 12, 6, and 8 oxygens for garnet, clinopyroxene, and plagioclase respectively. Fe^{3+} content has been calculated from charge balance for pyroxene and according to Droop (1987) for garnet. Amphibole structural formula has been calculated using the Amph-IMA Program with 23 oxygen and a normalization scheme according to Mogessie *et al*. (2004).

Garnet

Garnet is almandine- (Alm = 53-65 mol%), pyrope- (Prp = 15-25 mol%) and grossularite- rich (Grs = 15-26 mol%), with minor spessartine content (Sps ≤ 3 mol%). Compositional traverses and qualitative X-ray maps through some selected garnet crystals (Figs 5 & 6) reveal two different domains, a core and a rim, recognizable on the basis of their spessartine content, which is low and homogeneous in the core (Sps ≤ 1.3 mol%) and significantly higher in the rim (Sps ≥ 1.3 mol%). The thickness of the rim domain is generally < 100 μm (average of 65-75 μm), independent of garnet diameter (Fig. 6a). As a consequence, larger garnet porphyroblasts (> 1 mm in diameter) generally preserve a large core domain, whereas small garnet porphyroblasts (< 500 μm in diameter) eventually do not preserve any core domain. Garnet cores show a systematic decrease of grossularite counterbalanced by a slightly increase in pyrope from an inner core to an outer core (inner core: Grs_{22-26}, Prp_{17-20}; outer core: Grs_{18-23}, Prp_{20-23}). Garnet rims have a significant higher spessartine and almandine contents ($Sps_{1.3-3.0}$, Alm_{55-65}) and lower pyrope and grossularite (Prp_{15-25}, Grs_{15-23}) with respect to garnet core.

Pyroxene

Clinopyroxene inclusions in garnet (Cpx_1) is omphacite (Fig. 7a) with X_{Na} between 0.34 and 0.38, X_{Mg} between 0.69 and 0.79 and a low Fe^{3+} content (up to 0.10 a.p.f.u.) [X_{Na} = Na/(Na+Ca); X_{Mg} = Mg/(Mg+Fe)]. Compositional traverse through Cpx_1 included in garnet reveals a very thin rim characterized by a sharp decrease of Na (to X_{Na} ~ 0.10-0.14). Omphacite in the matrix shows a lower X_{Na} content (X_{Na}=0.25-0.30) than omphacite included in garnet, and a similar X_{Mg}. Clinopyroxene from the symplectite (Cpx_2) is diopside to augite (Fig. 7b) with Ca = 0.90-0.91 a.p.f.u., X_{Mg} between 0.70-0.80 and very low X_{Na} and Fe^{3+} content (X_{Na} = 0.03-0.06; Fe^{3+} = 0.00-0.08 a.p.f.u.). Orthopyroxene belongs to the enstatite-ferrosilite join (Fig. 7c). X_{Mg} ratio in orthopyroxene ranges from 0.51 to 0.54, the Al content is ~0.02 a.p.f.u. and Fe^{3+} content is between 0.03 and 0.13 a.p.f.u. No compositional difference has been observed between orthopyroxene in the rare symplectitic microstructures and orthopyroxene from the matrix.

Amphibole

All amphibole textural varieties, except cummingtonite, are calcic according to Leake *et al*. (1997). Amphibole inclusions in garnet (Am_1) are pargasite, aluminopargasite to magnesiohornblende with

Si = 5.87-6.00 a.p.f.u., Al = 2.60-3.49 a.p.f.u., Fe^{3+} = 0.1-0.5, and X_{Mg} = 0.59-0.61 (Fig. 7d,e). Amphibole replacing orthopyroxene (Am_2) is cummingtonite with X_{Mg}~0.7. Coronitic amphibole (Am_3) associated to coronitic plagioclase (Pl_2) is magnesiohornblende to pargasite with Si between 6.42 and 6.65 a.p.f.u. , Fe^{3+} between 0.35-0.42 and X_{Mg} ~0.63. Brownish to greenish amphibole in the rock matrix (Am_4), distinguished from Am_3 on microstructural basis, is zoned with a composition ranging between Mg-hornblende, pargasite to edenite and X_{Mg} ratio variable between 0.55 and 0.65. Amphibole (Am_5) replacing clinopyroxene is actinolite to ferroactinolite with X_{Mg} ranging between 0.45 and 0.55.

Plagioclase

Plagioclase associated to clinopyroxene in the symplectite (Pl_1) has oligoclase composition, ranging between Ab = 74-81 mol%. Plagioclase (Pl_1) associated to orthopyroxene shows a wider range of compositions (Ab ~73-91 mol%). Plagioclase from the kelyphites (Pl_2) shows an increase of Na content from the inner to the outer side of the corona (Ab=61-72 mol% to Ab=77-87 mol%, respectively). Plagioclase from the white pods is labradorite to andesine characterized by albite content in the range 42-61 mol%.

METAMORPHIC EVOLUTION CONSTRAINED BY MICROSTRUCTURES

The detailed interpretation of the microstructural features previously discussed for the garnet-pyroxene layers allows reconstruction of the metamorphic evolution of the studied samples in terms of their reaction history, i.e. in terms of reactants vs. products involved in the main prograde vs. retrograde reactions (Fig. 8).

Pre-symplectite stage

The earlier portion of the metamorphic history (pre-symplectite stage) (Fig. 8a) is recorded by mineral inclusion and compositional zoning of garnet porphyroblasts. Abundant omphacite (Cpx_1), rutile, quartz, epidote and amphibole (Am_1) inclusions in poikiloblastic garnet as well as the high jadeite content of omphacite (X_{Na} ratio up to 0.38) suggest that these minerals (Grt + Cpx_1 + Qtz + Rt) represent the stable assemblage corresponding to pre-symplectite eclogite-facies conditions. Euhedral amphibole (Am_1) and epidote only occur as inclusions in garnet and are therefore interpreted as prograde minerals. This eclogitic assemblage is also consistent with the occurrence of rare omphacite relicts in the matrix, pervasively replaced by the Cpx_2+Pl_1 symplectites. Although diffusion-controlled retrograde re-equilibration of garnet rims probably occurred (< 100 μm wide) as suggested by high Mn content (Sps ≥ 1.3 mol%), most of the garnet zoning is likely to represent the prograde path, at least in the larger porphyroblasts as discussed further in more detail. Garnet zoning shows a progressive increase in pyrope and a decrease in grossularite components from the inner core to the outer core (Figs 5 & 6), which is consistent with growth during increasing pressure and temperature and documented previously for other Variscan granulitized eclogites (e.g. O'Brien, 1997). How and why the prograde garnet zoning survived the pervasive high temperature overprint is discussed in the following sections.

Cpx_2+ Pl_1 and Opx+ Pl_1 ± Ilm symplectite/corona stage

This stage corresponds to the growth of two different symplectitic microstructures, namely the Cpx_2+Pl_1 and the Opx+Pl_1 symplectites (Fig. 8b). The Cpx_2+Pl_1 symplectites are more abundant, pervasively replacing omphacite in the matrix and locally also omphacite crystals included in garnet where these communicate with the matrix through fractures. Reaction modelling by the least square method (CSpace version 1.01, Djinn Works, Torres-Roldan *et al*., 2000) applied to the composition of Cpx_1 (omphacite), symplectitic plagioclase (Pl_1) and clinopyroxene (Cpx_2) from sample E9

(Table 1) yielded the following balanced reaction accounting for the formation of Cpx_2+Pl_1 symplectites, in agreement with Zhao *et al*. (2001) and Groppo *et al*. (2007a,b):

(1) 0.81 Cpx_1 + 0.05 Qtz → 0.55 Cpx_2 + 0.21 Pl_1

The Opx+Pl_1 symplectites are very rare and, being mostly surrounded by amphibole (Am_3), their relationships with both Cpx_2+Pl_1 symplectites and garnet are not unequivocal, although they always occur close to garnet porphyroblasts. Apart from the Opx+Pl_1 symplectites, orthopyroxene is commonly also found as (i) anhedral crystals (partially replaced by Am_3) at the outer margin of Pl_2+Am_3 coronae of garnet, and in contact with the former Cpx_1 (now replaced by Cpx_2+Pl_1 symplectites), and (ii) as more or less continuous Opx coronae isolating corroded quartz crystals from the former Cpx_1 (now replaced by Cpx_2+Pl_1 symplectites). Altogether, this evidence suggest that: firstly, both garnet and the omphacitic clinopyroxene Cpx_1 were likely involved in the orthopyroxene growth, whose occurrence at the outer margin of the Pl_2+Am_3 corona is probably a remnant of a former Opx+Pl_1 corona later replaced by the Pl_2+Am_3 assemblage (cf. Zhao *et al*., 2001); secondly, quartz and the Cpx_1 were likely involved in the orthopyroxene coronitic growth around quartz in the matrix. In both the cases, the orthopyroxene growth is roughly contemporaneous to the Cpx_2+Pl_1 symplectites development.

Considering the composition of omphacitic clinopyroxene (Cpx_1), garnet outer core (i.e. before the retrograde re-equilibrated rim), orthopyroxene and symplectitic plagioclase (Pl_1) from the same sample, the following balanced reactions can explain: (i) the development of Opx+Pl_1 coronae around garnet now almost completely replaced by the Pl_2+Am_3 assemblage plus the rare Opx+Pl_1 symplectites (reaction 2), and (ii) the occurrence of coronitic orthopyroxene around quartz relics in the matrix (reaction 3).

(2) 0.13 Grt + 0.78 Cpx_1 = 0.39 Pl_1 + 0.47 Opx

(3) 0.17 Grt + 0.06 Cpx_1 + 0.88 Qtz + = 0.31 Pl_1 + 0.30 Opx

At the outer margin of the Pl_2+Am_3 coronae of garnet, large anhedral ilmenite grains are present, surrounded and locally partially replaced by the Pl_2+Am_3 assemblage. Ilmenite occurs in a microstructural position similar to that of orthopyroxene, i.e. in between garnet and the former Cpx_1 (now replaced by Cpx_2+Pl_1 symplectites). Ilmenite and orthopyroxene, however, were never observed occurring together at the outer margin of the coronitic microstructures. This suggests that the ilmenite development could be related to a reaction involving garnet, the former omphacite and a Ti-rich phase (rutile), but not orthopyroxene. Considering the composition of garnet outer core (i.e. before the retrograde re-equilibrated rim), omphacitic clinopyroxene (Cpx_1), ilmenite, symplectitic plagioclase (Pl_1) and clinopyroxene (Cpx_2), the following balanced reaction can explain the presence of ilmenite in the coronitic structures:

(4a) 0.04 Grt + 0.79 Cpx_1 + 0.11 Rt = 0.24 Pl_1 + 0.54 Cpx_2 + 0.11 Ilm .

Both reactions (3) and (4) involve garnet and omphacitic clinopyroxene (Cpx_1) as reactants, and only differ from reaction (2) regarding the presence of quartz or rutile as additional reactant phases. Consequently, all these reactions probably occurred at the same *P-T* conditions as a function of variable compositions of micro-domains. In addition, combining reaction (4a) with reaction (1), the following balanced equilibrium may be obtained:

(4b) 0.05 Grt + 0.77 Cpx_1 + 0.07 Qtz + 0.12 Rt = 0.26 Pl_1 + 0.54 Cpx_2 + 0.12 Ilm

This more complete reaction explains the growth of both Cpx_2+Pl_1 symplectites and the Ilm+Pl_1 coronae between garnet and omphacite.

Pl_2+Am_3 corona stage

This stage is documented by the development of amphibole (Am_3) + plagioclase (Pl_2) assemblage at the expense of the former Opx_1+Pl_1± Ilm corona around garnet (Fig. 8c). Pl_2+Am_3 coronae commonly replace garnet, whereas coronitic amphibole usually replaces symplectitic Cpx_2 and

coronitic Opx and Ilm grains. These textures indicate that the Pl_2+Am_3 coronae postdate the Opx+Pl_1±Ilm coronae as already concluded by Zhao *et al*. (2001) for similar granulitized eclogites.

The growth of amphibole implies that H_2O was available in the system. However, the exclusive occurrence of Am_3 in coronitic microstructures suggests that H_2O was limited to these domains rather than pervading the whole rock. By combining the composition of garnet, original coronitic plagioclase (Pl_1), actual coronitic plagioclase (Pl_2) and amphibole (Am_3), the following balanced reaction may account for the development of the Pl_2+ Am_3 corona assemblage in intermediate positions between garnet and the original Opx+Pl_1 corona:

(5) 0.04 Grt + 0.70 Pl_1 + 0.01 H_2O = 0.72 Pl_2 + 0.01 Am_3.

Since Am_4 has a chemical composition similar to that of Am_3 and has been distinguished only on microstructural basis, the growth of Am_4 in the matrix should be ascribed to the same metamorphic stage.

Late stage metamorphic evolution

The later stage of metamorphic evolution is documented by the local growth of actinolite, chlorite, very minor epidote and titanite in the rock matrix. Syn-D_4 biotite growth along shear bands is also tentatively attributed to this stage for which Franceschelli *et al*. (1998) estimated *P-T* conditions of ~300-400 °C and < 0.2-0.3 GPa.

METAMORPHIC EVOLUTION CONSTRAINED USING THE *P-T* PSEUDOSECTION APPROACH

The *P-T* pseudosections have been calculated in the NCKFMASTH system using Perple_X (Connolly, 1990; 2009). Details of the calculation are given in the Appendix section. A detailed description of the topology of each pseudosection is considered beyond the scope of this article, therefore the variance of each field as well as the complete set of compositional isopleths and isomodes are provided as supplementary material.

Modelling the pre-symplectite stage

Microstructural features described above suggest that the pre-symplectite equilibrium assemblage (Grt + Cpx_1 + Qtz + Rt ± Am_1) pervasively grew throughout sample E9, and therefore that the earlier portion of the *P-T* evolution can be modelled based on the bulk composition measured by XRF (Table 2). The corresponding *P-T* pseudosection is shown in Fig. 9.

Based on the observed vs. modelled mineral compositions, the following *P-T* conditions are obtained:

i) An early prograde stage is constrained by the composition of Cpx_1 (preserved as inclusions in garnet: X_{Na}=0.34) and garnet inner core (Grs=22-26 mol%; Prp=17-20 mol%) at 660-680°C and 1.6-1.8 GPa. The equilibrium assemblage modelled at these *P-T* conditions (i.e. Cpx + Grt + Qtz + Am + Qtz + Rt + Bt, with biotite < 1.5 vol%) is consistent with most of the petrographic observations.

ii) A later prograde stage is constrained by the composition of outer cores of garnets (Grs= 18-23 mol%; Prp=20-23 mol%), as well as by Cpx_1 composition (omphacite inclusions are also preserved in the outer garnet core: X_{Na}=0.34) at 660-700°C and 1.7-2.1 GPa. These *P-T* conditions lie inside the same four-variant Cpx + Grt + Qtz + Am + Qtz + Rt + Bt field of the earlier prograde stage, but closer to the upper boundary of the amphibole stability field.

The overall *P-T* evolution modelled by the *P-T* pseudosection of Fig. 9 is therefore characterized by a prograde increase in both *P* and *T* from about 600°C, 1.0 GPa to 690°C, 1.9 GPa. However, since the garnet rim shows evidence of a diffusion-controlled retrograde re-equilibration (i.e. the original rim composition is no more available), peak *P-T* conditions could have been

slightly higher than that here modeled, more likely in the amphibole-absent five-variant Cpx + Grt + Qtz + Rt + Bt field.

Modelling the symplectite and corona stages

The metamorphic stages following the eclogite-facies peak-*P* conditions are characterized by the widespread development of symplectites, coronae and kelyphites. These microstructures are the results of metamorphic reactions occurring at the scale of small domains, not represented by whole-rock composition. In order to model *P-T* conditions, the method of Groppo *et al*. (2007a, b) was applied (see also Cruciani *et al*., 2008, 2011) for calculating the composition of the effectively reacting microdomains that were involved in the formation of symplectites and coronae based on mineral compositions in sample E9 (Table 1) and the stoichiometric coefficients of the previously deduced balanced reactions (2) to (5). Different *P-T* pseudosections (compositions in Table 2) representative of the developed microstructures were then calculated as detailed below.

i) *Opx+Pl$_1$ symplectite/corona* – These microstructures were modelled using the effective bulk composition obtained from reaction (2). The calculated *P-T* pseudosection, reported in Fig. 10a, shows that the equilibrium (2) is a continuous reaction that occurred across a relatively large *P-T* interval, at > 800°C. Moving along a decompression path from about 1.7 GPa to 1.0 GPa, garnet and clinopyroxene are consumed (ΔGrt = -13 vol%; ΔCpx = -9 vol%), whereas plagioclase and orthopyroxene are produced (ΔPl = +14 vol%; ΔOpx = +10 vol%), consistent with the predictions of reaction (2). The *P-T* conditions at which the Opx+Pl$_1$ symplectites and coronae grew are further constrained by the Pl$_1$ (X_{Na}=0.74-0.78) and orthopyroxene (X_{Mg}=0.51-0.54) compositions at > 800°C, and 1.0-1.3 GPa (Fig. 10a).

ii) *Cpx$_2$+Pl$_1$ symplectite and Ilm+Pl$_1$ coronae* – The effective bulk composition used to model these microstructures was obtained from the balanced reaction (4a), whose reactants are the same as in reaction (2) except for rutile. The appearance of ilmenite at the expenses of rutile (in the presence of garnet and clinopyroxene) occurs in a relatively narrow *P*-interval at > 800°C. Passing from the rutile-bearing (and ilmenite-absent) fields at 1.5 GPa to the ilmenite-bearing (and rutile-absent) field at 0.8 GPa, garnet, clinopyroxene and rutile are consumed (ΔGrt = -10 vol%; ΔCpx = -12 vol%; ΔRt = -4 vol%) and plagioclase and ilmenite are produced (ΔPl = +17 vol%, ΔIlm = +6 vol%), in agreement with the predictions of reaction (4a). Plagioclase composition (X_{Na}=0.74-0.78) further constrains the *P-T* conditions at > 800°C and 0.9-1.2 GPa (Fig. 10b).

iii) *Pl$_2$+Am$_3$ corona* – The growth of the Pl$_2$+Am$_3$ assemblage has been modelled using the effective bulk composition obtained from the balanced reaction (5). In the calculated pseudosection (Fig. 10c) this continuous reaction occurs on a large *P*-interval at > 650°C. The calculated plagioclase (X_{Na} = 0.62-0.68) and amphibole (Si = 6.4-6.6 a.p.f.u.; X_{Mg} = 0.61-0.63) compositional isopleths provide further *P-T* constraints on the formation of Pl$_2$+Am$_3$ corona, modelled at 730-830°C, and 0.8-1.1 GPa (Fig. 10c). Moving along a decompression path in this *P-T* range, garnet is consumed (ΔGrt = -2 vol%), whereas plagioclase and amphibole (ΔAm = +3 vol%; ΔPl = +1 vol%) are produced, in agreement with microstructural evidence. The progression of reaction (5) led to the formation of white pods (Fig. 4d) that widespread occur in the Am-Pl layers (Fig. 2d).

DISCUSSION

Attainment of equilibrium on a domainal scale and preservation of the prograde history

Microstructural evidence and the results of thermodynamic modelling both show that sample E9 experienced a complex polyphase metamorphic history characterized by a prograde HP eclogite-facies event followed by a HT granulite-facies stage. A temperature increase of about 150°C occurred during decompression from ~ 2.0 GPa to ~ 1.0 GPa.

Reconstruction of the pre-granulitic history was possible thanks to the preservation not only of the prograde HP microstructures, but also of the garnet prograde compositions, in spite of the

widespread HT overprint. In particular, garnet compositional maps show that, apart from a ~100 μm wide Mn-rich rim likely due to retrograde, diffusion controlled, re-equilibration and resorption, garnet cores preserve a well documented zoning coherent with its prograde growth at increasing pressure and temperature (i.e. Grs decreases and Prp increases from the inner to the outer core). Although the standard types of diffusion models predict that the prograde garnet zoning should be mostly reset during heating at > 700°C (e.g. Caddick *et al*., 2010), O'Brien (1997) first documented the possibility of garnet preserving its prograde compositional profile in granulitized eclogites from the Bohemian Massif. Since then, several other studies have reported examples of preserved prograde garnet zoning at high temperatures (e.g. O'Brien *et al*., 1997; Zhao *et al*., 2001; Štípská & Powell, 2005; Medaris *et al*., 2006; Groppo *et al*., 2007a, 2012; Cruciani *et al*., 2011). The samples studied by O'Brien (1997) are characterized by abundant symplectitic and coronitic microstructures similar as described here for sample E9 and also implying attainment of equilibrium only at the scale of microdomains. This led O'Brien (1997) to suggest that grain boundary diffusion and material transport have a major influence on the development of diffusion zoning and that slow grain boundary diffusion could invalidate the standard types of diffusion models.

In the specific case of sample E9, calculated H_2O (wt%) isomodes (Fig. 11a) show that the amount of water available in the system progressively decreases from ~ 1.4 wt% at ~ 600°C to < 0.1 wt% at the eclogite-facies peak-*P* conditions (i.e. the system was H_2O-saturated during its prograde evolution; Guiraud *et al*., 2001). Approximately at peak-*P* conditions, the *P-T* trajectory becomes tangential to the H_2O isomodes, thus implying that the mineral assemblage was H_2O under-saturated during the subsequent evolution, i.e. metamorphic reactions could not proceed until H_2O-saturated conditions were again reached or, alternatively, H_2O was introduced from outside. Sample E9 remained H_2O-undersaturated during heating and decompression up to ca. 800°C at 1.5 GPa, when the *P-T* path becomes tangential to an H_2O content contour (Fig. 11a) (see Guiraud *et al*., 2001 for the interpretation of H_2O-saturated vs. H_2O-undersaturated conditions). Along the subsequent heating and decompression path, the system became again slightly H_2O-saturated (i.e. the P-T path intersects the H_2O isomode contours towards decreasing values, despite the overall H_2O content being extremely low), thus allowing the development of coronitic and symplectitic microstructures within very local domains. Fig. 11a shows that during cooling and further decompression, sample E9 was again H_2O-undersaturated (i.e. the *P-T* path intersects the H_2O isomode contours toward increasing values of H_2O content), thus implying that metamorphic reactions could have operated along this portion of the *P-T* path only if H_2O was introduced from outside. Consequently, the growth of amphibole in the Pl_2+Am_3 assemblage at the expense of the former Opx+Pl_1 coronae and in the rock matrix (Am_4) required an external fluid. Depending on the amount of introduced H_2O and hence, on the longer or shorter persistence of H_2O-saturated conditions, the Pl_2+Am_3 corona and the Am_4 in the matrix could have developed at different scales, ranging from the thin (70-300 μm) Pl_2+Am_3 coronae around garnet of the garnet-pyroxene layers, to the widespread plagioclase + amphibole assemblage observed in the "white pods" of the amphibole-plagioclase layers. These layers thus represent different hydration degrees of the eclogitic assemblage by migrating fluids in agreement with the observation of Franceschelli *et al.* (2007) of a late-stage "amphibolitization front" crosscutting the regional foliation.

The *P-T* pseudosection approach applied on non-equilibrated samples: a challenging analysis

The concept of equilibration volume, i.e. the scale on which it is plausible to suggest that the minerals were in equilibrium with each other (e.g. Powell & Holland, 2008), plays a crucial role for thermobarometry involving pseudosections, because the chemical composition of the equilibration volume is the starting point for the calculations. Therefore, the application of the pseudosection approach to a clearly non-equilibrated sample, such as the studied granulitized eclogite E9, would seem not recommendable. On the other hand, it is the non-equilibrated nature of the sample that

allows the calculation of the equilibria relevant for the development of coronitic and symplectitic microstructures, because both the reactants and the products are still preserved. The challenge of this study has been to exploit the unique possibility offered by such microstructures for calculating balanced reactions between reactants and products at different stages of the metamorphic path, to constrain the composition of effectively reacting microdomains in which symplectites and coronae grew, and to construct corresponding pseudosections and determine *P-T* conditions.

This study demonstrates that the bulk compositions calculated by combining mineral compositions of both reactants and products with the stoichiometric coefficients of the balanced reactions are representative of the effectively reacting symplectitic and coronitic micro-domains. The results of the pseudosection calculation may be considered reliable if the modelled isomodes and compositional isopleths are consistent with both the observed mineral assemblages/compositions and the inferred equilibria. Furthermore, if some of the domainal microstructures show mutual relationships suggesting their contemporaneous growth (such as the Opx+Pl_1 and the Ilm+Pl_1 coronae), the *P-T* constraints obtained from the two different pseudosections should be the same. The latter provides an important additional test for the reliability of pseudosection results.

Comparison with other Sardinian eclogites

The *P-T* path of the Punta de li Tulchi granulitized eclogite (Fig. 11a) is markedly similar to the paths deduced for retrogressed eclogites from the Migmatite Complex (Axial Zone) at Golfo Aranci (Giacomini *et al*., 2005a) and for the Punta Orvili metabasite (Cruciani *et al*., 2011) (Fig. 11b). The latter is assumed to belong to the Low to Medium Grade Metamorphic Complex (Nappe Zone), because it crops out very close to the Posada-Asinara shear zone (Fig. 1); the retrogressed eclogite there has a different bulk composition and lacks orthopyroxene (e.g. Franceschelli *et al*., 1998; Cruciani *et al*., 2011).

The first portion of the *P-T* path for the three retrogressed eclogites consists of a prograde increase of both *P* and *T* to eclogite-facies peak conditions (1.9-2.1 GPa, 600-700°C). After the eclogite stage, they underwent significant re-equilibration under granulite-facies conditions (700-800°C, 1.0-1.2 GPa), followed by high-*T* amphibolite-facies metamorphism (650-800°C; 0.7-1.0 GPa). Comparing the *P-T* paths calculated at the same aH_2O for the eclogites from the three different localities (Fig. 11b), it appears that the Punta de li Tulchi eclogite records peak temperatures about 40-50°C higher than those of Golfo Aranci retrogressed eclogite and 90-100°C higher as those of Punta Orvili metabasite. However, changing aH_2O shifts the whole *P-T* trajectories towards lower or higher temperatures (e.g. lowering aH_2O from 1.0 to 0.5 results in a shift of about 50°C toward lower *T*; compare Fig. 11a and Fig. 11b). It is therefore difficult to assess whether the different modelled peak-*T* for the three localities reflect true differences in temperatures, and/or are due to different aH_2O. Independent of the absolute *P-T* values registered by the Golfo Aranci, Punta Orvili and Punta de li Tulchi eclogites, however, it is worth nothing that their *P-T* evolutions are very similar in shape, thus suggesting a common tectonic scenario for their evolution.

The new data presented for the Punta de li Tulchi granulitized eclogite are substantially in agreement with the geodynamic scenario proposed by Cruciani *et al.* (2011) for the evolution of the NE Sardinia eclogites. According to these authors the prograde evolution of the eclogites took place under a geothermal gradient of ~10°C km^{-1}, compatible with a relatively hot subduction of a small, young marginal basin rather than with the prolonged subduction of a wider more thermally mature oceanic plate. The subsequent increase of the geothermal gradient to 25-30°C km^{-1} marks the beginning of the Variscan continental collision. The following exhumation of the granulitized eclogites to relatively shallow crustal levels, was accompanied by re-equilibration under granulite-

to HT amphibolite-facies conditions, most likely during a period of protracted continental collision.

ACKNOWLEDGEMENTS

Microprobe analyses have been carried out with the assistance of M. Serracino (IGAG–CNR, Roma). This work was funded by Progetti di Ricerca Locale, Cagliari University funds. We are grateful to the reviewers Ricardo Arenas and Mike Rubenach for their helpful comments and criticism. Domingo Aerden and Doug Robinson are thanked for their editorial handling and improving the text.

REFERENCES

Berger, J., Féménias, O., Ohnenstetter, D., Plissart, G. & Mercier, J.-C.C., 2010. Origin and tectonic significance of corundum-kyanite-sapphirine amphibolites from the Variscan French Massif Central. *Journal of Metamorphic Geology*, **28**, 341 – 360.

Caddick, M.J., Konopásek, J. & Thompson, A.B., 2010. Preservation of garnet growth zoning and the duration of prograde metamorphism. *Journal of Petrology*, **51,** 2327-2347.

Carmignani, L., Oggiano, G., Barca, S., Conti, P., Salvadori, I., Eltrudis, A., Funedda, A. & Pasci, S., 2001. Geologia della Sardegna. Note illustrative della Carta Geologica della Sardegna a scala 1:200000. *Memorie descrittive della Carta Geologica d'Italia*, **60**, 283 pp.

Carosi, R. & Palmeri, R., 2002. Orogen-parallel tectonic transport in the Variscan belt of northeastern Sardinia (Italy): implications for the exhumation of medium-pressure metamorphic rocks. *Geological Magazine*, **139**, 497-511.

Connolly, J.A.D., 1990. Multivariable phase diagrams: an algorithm based on generalized thermodynamics. *American Journal of Science*, **290**, 666 – 718.

Connolly, J.A.D., 2009. The geodynamic equation of state: what and how. *Geochemistry, Geophysics, Geosystems*, **10**, Q10014.

Cortesogno, L., Gaggero, L., Oggiano, G. & Paquette, J.-L., 2004. Different tectono-thermal evolutionary paths in eclogitic rocks from the axial zone of the Variscan chain in Sardinia (Italy) compared with the Ligurian Alps. *Ofioliti*, **29**, 125 – 144.

Cruciani, G., Franceschelli, M. & Groppo, C., 2011**.** *P-T* evolution of eclogite-facies metabasite from NE Sardinia, Italy: insights into the prograde evolution of Variscan eclogites. *Lithos*, **121**, 135 – 150.

Cruciani, G., Franceschelli, M., Groppo, C., Brogioni, N. & Vaselli, O., 2008. Formation of clinopyroxene + spinel and amphibole + spinel symplectites in coronitic gabbros from the Sierra de San Luis (Argentina): a key to post-magmatic evolution. *Journal of Metamorphic Geology*, **26**, 759 – 774.

Dale, J., Powell, R., White, R.W., Elmer, F.L. & Holland, T.J.B., 2005. A thermodynamic model for Ca-Na clinoamphiboles in Na_2O – CaO – FeO – MgO – Al_2O_3 – SiO_2 – H_2O – O for petrological calculations. *Journal of Metamorphic Geology*, **23**, 771 – 791.

Droop, G.T.R., 1987. A general equation for estimating Fe^{3+} concentration in ferromagnesian silicates and oxides from microprobe analyses, using stoichiometric criteria. *Mineralogical Magazine*, **51**, 431-435.

Elter, F.M., Franceschelli, M., Ghezzo, C., Memmi, I. & Ricci, C.A., 1986. The geology of northern Sardinia. In: Carmignani, L., Cocozza, T., Ghezzo, C., Pertusati, P.C., Ricci, C.A. (Eds.), Guide-Book to the Excursion on the Paleozoic Basement of Sardinia. IGCP Project. Newsletter, **5**, 87–102.

Elter, F.M., Padovano, M. & Kraus, R.K., 2010. The emplacement of Variscan HT metamorphic rocks linked to the interaction between Gondwana and Laurussia: structural constraints in NE Sardinia (Italy). *Terra Nova*, **22**, 369 – 377.

Elter, F.M. & Pandeli, E., 2005. Structural-metamorphic correlations between three Variscan segments in southern Europe: Maures Massif (France), Corsica(France)-Sardinia(Italy), and Northern Appennines (Italy). In: Carosi, R., Dias, R., Iacopini, D., and Rosenbaum, G. (Eds.) The Southern Variscan belt. *Journal of the Virtual Explorer*, **19**, Paper 1.

Ferrando, S., Lombardo, B. & Compagnoni, R., 2008. Metamorphic history of HP mafic granulites from the Gesso-Stura Terrain (Argentera Massif, Western Alps, Italy). *European Journal of Mineralogy*, **20**, 777 – 790.

Fettes, D. & Desmons, J., 2007. Metamorphic rocks- A classification and glossary of terms. Cambridge University Press, Cambridge, 244 pp.

Franceschelli, M., Eltrudis, A., Memmi, I., Palmeri, R. & Carcangiu, G., 1998. Multi-stage metamorphic re-equilibration in eclogitic rocks from the Hercynian basement of NE Sardinia (Italy). *Mineralogy and Petrology*, **62**, 167-193.

Franceschelli, M., Puxeddu, M. & Cruciani, G., 2005. Variscan metamorphism in Sardinia, Italy: review and discussion. In: Carosi, R., Dias, R., Iacopini, D., Rosenbaum, G. (Eds.) The Southern Variscan belt. *Journal of the Virtual Explorer*, **19**, Paper 2.

Franceschelli, M., Puxeddu, M., Cruciani, G. & Utzeri, D., 2007. Metabasites with eclogites facies relics from Variscides in Sardinia, Italy: a review. *International Journal of Earth Sciences*, **96**, 795 – 815.

Giacomini, F., Bomparola, R.M. & Ghezzo, C., 2005a. Petrology and geochronology of metabasites with eclogite facies relics from NE Sardinia: constraints for the Palaeozoic evolution of Southern Europe. *Lithos*, **82**, 221-248.

Giacomini, F., Bomparola, R.M. & Ghezzo, C., 2005b. The pre-Variscan magmatic-sedimentary history in the high-grade metamorphic basement of northern Sardinia (Italy): constraints from U/Pb geochronology and geochemistry. Epitome. Geoitalia 2005, Quinto Forum Italiano di Scienze della Terra. Spoleto, 21 – 23 settembre 2005.

Giacomini, F., Bomparola, R.M., Ghezzo, C. & Guldbransen, H., 2006. The geodynamic evolution of the Southern European Variscides: constraints from the U/Pb geochronology and geochemistry of the Lower Palaeozoic magmatic-sedimentary sequences of Sardinia (Italy). *Contributions to Mineralogy and Petrology*, **152**, 19-42.

Giacomini, F., Dallai, L., Carminati, E., Tiepolo, M. & Ghezzo, C., 2008. Exhumation of a Variscan orogenic complex: insights into the composite granulitic-amphibolitic metamorphic basement of south-east Corsica (France). *Journal of Metamorphic Geology*, **26**, 403 – 436.

Green, E.C.R., Holland, T.J.B. & Powell, R., 2007. An order-disorder model for omphacitic pyroxenes in the system jadeite-diopside-hedenbergite-acmite, with applications to eclogitic rocks. *American Mineralogist*, **92**, 1181 – 1189.

Groppo, C., Lombardo, B., Rolfo, F. & Pertusati, P.C., 2007a. Clockwise exhumation path of granulitized eclogites from the Ama Drime range (Eastern Himalayas). *Journal of Metamorphic Geology*, **25**, 51-75.

Groppo, C., Lombardo, B., Castelli, D. & Compagnoni, R., 2007b. Exhumation history of the UHPM Brossasco-Isasca Unit, Dora-Maira Massif, as inferred from a phengite-amphibole eclogite. *International Geology Review*, 49, 142-168.

Guiraud, M., Powell, R. & Rebay, G., 2001. H_2O in metamorphism and the preservation of metamorphic mineral assemblages. *Journal of Metamorphic Geology*, **19**, 445 – 454.

Helbing, H., Frisch, W. & Bons, P.D., 2006. South Variscan terrane accretion: Sardinian constraints on the intra-Alpine Variscides. Journal of Structural Geology, **28**, 1277-1291.

Helbing, H. & Tiepolo, M., 2005. Age determination of Ordovician magmatism in NE Sardinia and its bearing on Variscan basement evolution. *Journal of the Geological Society of London*, **162**, 689-700.

Holland, T.J.B. & Powell, R., 1996. Thermodynamics of order-disorder in minerals: II. Symmetric formalism applied to solid solutions. *American Mineralogist*, **81**, 1425 – 1437.

Holland, T.J.B. & Powell, R., 1998. An internally consistent thermodynamic data set for phases of petrological interest. *Journal of Metamorphic Geology*, **16**, 309 – 343.

Holland, T.J.B., Baker J.M. & Powell, R., 1998. Mixing properties and activity-composition relationships of chlorites in the system MgO-FeO-Al_2O_3-SiO_2-H_2O. *European Journal of Mineral*ogy, **10**, 395 – 406.

Lardeaux, J.M., Ledru, P., Daniel, I. & Duchene, S., 2001. The Variscan French Massif Central-a new addition to the ultra-high pressure metamorphic 'club': exhumation processes and geodynamic consequences. *Tectonophysics*, **332**, 143 – 167.

Leake, B.E., Woolley, A.R., Arps, C.E.S., Birch, W.D., Gilbert, M.C., Grice, J.D., Hawthorne, F.C., Kato, A., Kisch, H.J., Krivivichev, V.G., Linthout, K., Laird, J., Mandarino, J.A., Maresch, W.V., Nickel, E.H., Rock, N.M.S., Schumacher, J.C., Smith, D.C., Stephenson, N.C.N., Ungaretti, L., Whittaker, E. & Youzhi, G., 1997. Nomenclature of amphiboles: report of the subcommittee on amphiboles of the International Mineralogical Association, commission on new minerals and mineral names. *The Canadian Mineralogist*, **35**, 219-246.

Massonne, H.-J., 2001. First find of coesite in the ultrahigh-pressure metamorphic area of the central Erzgebirge, Germany. *European Journal of Mineralogy*, **13**, 565-570.

Medaris, L.G., Ghent, E.D., Wang, H.F., Fournelle, J.H. & Jelínek, E., 2006. The Spaciche eclogite: constraints on the *P-T*-t history of the Gföhl granulite terrane, Moldanubian Zone, Bohemian Massif. *Mineralogy and Petrology*, **86**, 203 – 220.

Miller, C., Sassi, F.P. & Armari, G., 1976. On the occurrence of altered eclogitic rocks in north-eastern Sardinia and their implication. *Neues Jahrbuch für Geologie und Paläontologie-Monatshefte*, **11**,683-689.

Mogessie, A., Ettinger, K. & Leake, B.E., 2004. AMPH-IMA04 a revised Hypercard program to determine the name of an amphibole from chemical analyses according to the 2004 International Mineralogical Association scheme. *Mineralogical Magazine*, **68**, 825 – 830.

Morimoto, N., 1988. Nomenclature of Pyroxenes. *Mineralogy and Petrology*, **39**, 55-76.

Nakamura, D., Svojtka, M., Naemura, K. & Hirajima, T., 2004. Very high-pressure (> 4 GPa) eclogite associated with the Moldanubian Zone garnet peridotite (Nove Dvory, Czech Republic). *Journal of Metamorphic Geology*, **22**, 593-603.

Nasdala, L. & Massonne, H.-J., 2000. Microdiamonds from the Saxonian Erzgerbirge, Germany: in situ micro-raman characterisation. European Journal of Mineralogy, **12**, 495 – 498.

Newton, R.C., Charlu, T.V. & Kleppa, O.J., 1981. Thermochemistry of the high structural state plagioclases. *Geochimica et Cosmochimica Acta*, **44**, 933 – 941.

O'Brien, P.J., 1997. Garnet zoning and reaction textures in overprinted eclogites, Bohemian Massif, European Variscides: A record of their thermal history during exhumation. *Lithos*, **41**, 119-133.

O'Brien, P.J., 2008. Challenges in high-pressure granulite metamorphism in the era of pseudosections: reactions textures, compositional zoning and tectonic interpretation with examples from the Bohemian Massif. *Journal of Metamorphic Geology*, **26**, 235 – 251.

O'Brien, P.J., Kröner, A., Jaeckel, P., Hegner, E., Żelażniewicz, A. & Kryza., R., 1997. Petrological and isotopic studies on Palaeozoic high-pressure granulites, Góry Sowie Mts, Polish Sudetes. *Journal of Petrology*, **38**, 433-456.

O'Brien, P.J. & Rötzler, J., 2003. High-pressure granulites: formation, recovery of peak conditions and implications for tectonics. *Journal of Metamorphic Geology*, **21**, 3 – 20.

O'Brien, P.J. & Ziemann, M.A., 2008. Preservation of coesite in exhumed eclogite: insights from Raman mapping. *European Journal of Mineralogy*, **20**, 827-834.

Palmeri, R., Fanning, M., Franceschelli, M., Memmi, I., Ricci, C.A., 2004. SHRIMP dating of zircons in eclogite from the Variscan basement in north-eastern Sardinia (Italy). *Neues Jahrbuch für Mineralogie - Monatshefte*, **6**, 275-288.

Powell, R. & Holland, T.J.B., 2008. On thermobarometry. *Journal of Metamorphic Geology*, **26**, 155 – 179.

Racek, M., Štípská, P., Pitra, P., Schulmann, K. & Lexa, O., 2006. Metamorphic record of burial and exhumation of orogenic lower and middle crust: new tectonothermal model for the Drosendorf window (Bohemian Massif). *Mineralogy and Petrology*, **86**, 221-251.

Rötzler, J. & Romer, R.L., 2001. *P-T*-t evolution of ultrahigh-temperature granulites from the Saxon Granulite Massif, Germany. Part I: Petrology. *Journal of Petrology*, **42**, 1995 – 2013.

Štîpská, P. & Powell, R., 2005. Constraining the *P-T* path of a MORB-type eclogite using pseudosections, garnet zoning and garnet-clinopyroxene thermometry: an example from the Bohemian Massif. *Journal of Metamorphic Geology*, **23**, 725–743.

Štîpská, P., Pitra, P. & Powell, R., 2006. Separate or shared metamorphic histories of eclogites and surrounding rocks? An example from the Bohemian Massif. *Journal of Metamorphic Geology*, **24**, 219-240.

Tajčmanová, L., Konopásek, J. & Schulmann, K., 2006. Thermal evolution of the orogenic lower crust during exhumation within a thickened Moldanubian root of the Variscan belt of Central Europe. *Journal of Metamorphic Geology*, **24**, 119 – 134.

Torres-Roldan, R.L., García-Casco, A. & García-Sanchez, P.A., 2000. CSpace: an integrated workplace for the graphical and algebraic analysis of phase assemblages on 32-bit wintel platforms. *Computers & Geosciences*, **26**, 779 - 793.

Willner, A.P., Rötzler, K. & Maresch, W., 1997. Pressure-temperature and fluid evolution of quartzo-feldspathic metamorphic rocks with a relic high-pressure granulite-facies history from the Central Erzgebirge (Saxony, Germany). *Journal of Petrology*, **38**, 307 – 336.

Zhao, G., Cawood, P.A., Wide ,S.A. & Lu, L., 2001. High-pressure granulites (retrograded eclogites) from the Hengshan Complex, North China Craton: petrology and tectonic implications. *Journal of Petrology*, **42**, 1141 – 1170.

APPENDIX

Pseudosection calculation.

The phases considered in the modeling are: amphibole, biotite, white mica, clinopyroxene, orthopyroxene, garnet, plagioclase, zoisite/clinozoisite, ilmenite, rutile, quartz, chlorite and titanite. Solid solution models are: Holland *&* Powell (1998) for garnet and white mica, Holland *&* Powell (1996) for orthopyroxene, Green *et al*. (2007) for clinopyroxene, Holland *et al*. (1998) for chlorite, Dale *et al*. (2005) for amphibole and Newton *et al*. (1981) for plagioclase. All iron is considered as bivalent because all the phases have negligible Fe^{3+}, and the very rare (<< 1 vol%) Fe^{+3}-bearing epidote inclusions within garnet core are interpreted as prograde relics.

Mn has not been considered in the calculation, because its content in garnet is very low and homogeneous and it mainly enters in the diffusion-controlled retrograde rim of garnet. All the pseudosections have been calculated at $a H_2O$=1.0. However, the effects, on the pseudosection topologies, of a lower $a H_2O$ have been also investigated. Lowering the $a H_2O$ results in a general shift of all the field boundaries and compositional isopleths toward lower temperatures. In particular, a shift of about 30-40°C is observed if the $a H_2O$ is set at 0.5.

FIGURE CAPTIONS

Fig. 1. (a): Geological sketch map of NE Sardinia coast. (b): Main structural elements of the Variscan chain of Sardinia from Carmignani *et al*. (2001). PAL: Posada-Asinara Line. (c): Sketch map of Punta de li Tulchi area.

Fig. **2**. Field photographs of Punta de li Tulchi granulitized eclogite. (a): Alternation of decimeter-scale (GP) Grt-Px layers and (AP) Am-Pl layers; (b): Grt-Px layers showing millimetric S_2 oriented clinopyroxene + plagioclase symplectites and garnet porphyroblasts. Grt-Px layers show a decrease in crystal size resembling mylonite (M). (c): Detail of the Grt-Px layer shown in Fig. 2b (rectangle). Reddish garnet crystals with a dark corona are surrounded by the clinopyroxene + plagioclase symplectite (white). (d): White pods (WP) in the Am-Pl layers elongated as the S_3 schistosity. The S_3 schistosity is cut by millimeter-scale shear bands.

Fig. 3. Photomicrographs and BSE images showing the relevant microstructures of the Punta de li Tulchi granulitized eclogites. (a) Overview of the granulitized eclogite (sample E9). Coronitic garnet set in a Cpx_2+Pl_1 symplectite matrix. Grt-Px layer. Plane Polarized Light (PPL). (b) Coronitic garnet with inclusions of omphacite (Cpx_1), rutile and amphibole (Am_1). Quartz is also included in Cpx_1. Grt-Px layer. BSE image. (c) Detail of Am_1, rutile and quartz inclusions in garnet. Grt-Px layer. BSE Image. (d) Detail of Cpx_2+Pl_1 symplectite matrix around garnet. Orthopyroxene occurs in the matrix and at the interface between the Pl_2+Am_3 corona and the Cpx_2+Pl_1 symplectite. Grt-Px layer. BSE image. (e) Rare Opx + Pl_1 symplectite preserved in a Grt-Px layer sample. Cpx_2+Pl_1 and Opx+Pl_1 symplectites are surrounded by matrix amphibole (Am_4). BSE image. (f) Detail of orthopyroxene at the interface between Cpx_2+Pl_1 symplectite and Am_3+Pl_2 kelyphite. Orthopyroxene is partially replaced by cummingtonite. Grt-Px layer. BSE image.

Fig. 4. Photomicrographs and BSE images showing the relevant microstructures of the Punta de li Tulchi granulitized eclogites. (a) Corona around garnet made up of plagioclase (Pl_2), amphibole (Am_3) and anhedral ilmenite. Grt-Px layer. PPL. (b) Quartz grain surrounded by orthopyroxene and Cpx_2 clinopyroxene. The contact between quartz and pyroxenes is marked by a cummingtonite layer. Grt-Px layer, BSE image. (c) Medium-grained matrix amphibole (Am_4) showing a pale green core surrounded by a brownish discontinuous rim. Grt-Px layer. PPL. (d) Microstructural features of layers containing white pods of amphibole and plagioclase (Am-Pl layers). PPL.

Fig. 5. Compositional variations of garnet core and rim in mol%. (a) pyrope vs. spessartine. (b) grossularite vs. spessartine. (c) almandine vs. spessartine. Additional garnet analyses not reported in Tables 1,S1 are also shown.

Fig. 6. (a) Schematic sketch of garnet zoning and kelyphite microstructure (redraw of Fig. 3b). (b) Zoning profile of garnet from Fig. 3b. The trace of the profile is shown in Fig. 6a.

Fig. 7. (a), (b), (c) Clinopyroxene and orthopyroxene classification in the (Wo+En+Fs)-Jd-Ae and Wo-En-Fs diagrams (Morimoto, 1988). (d), (e) Ca-amphibole classification in the diagram after Leake *et al*. (1997). All textural types of amphiboles are reported. Additional pyroxene and amphibole analyses not reported in Tables 1, S1, S2 are also shown.

Fig. 8. Microstructure and reaction history of sample E9. (a) pre-symplectite eclogitic stage; (b) Cpx_2+Pl_1 and Opx+Pl_1 symplectite/corona stage; (c) Am_3+Pl_2 corona stage. Fig. 8c is a redraw of part of the microstructure shown in Fig. 3d.

Fig. 9. (a) *P–T* pseudosection (NCKFMASTH system) calculated at $aH_2O = 1$ for the bulk composition of Grt-Px layer sample E9 (compositions in Table 2). White, light-, medium-, and dark-grey fields are di-, tri-, quadri-, and penta-variant fields, respectively. Dotted ellipses represent

P-T conditions for pre-symplectite stages estimated using clinopyroxene (b) and garnet (c,d) compositional isopleths.

Fig. 10. *P–T* pseudosections in the NCKFMASTH system calculated at $aH_2O = 1$ for the bulk compositions of the effectively reacting microdomains (Table 2). White, light-, medium-, and dark-grey fields are di-, tri-, quadri-, and penta-variant fields, respectively. Dotted ellipses in (a), (b), (c) represent the inferred *P-T* conditions of formation of $Opx+Pl_1$ corona/symplectite, $Ilm+Pl_1$ corona, and Am_3+Pl_2 corona, respectively, estimated using plagioclase, orthopyroxene and amphibole compositional isopleths. Some relevant modal abundances (vol.%) of garnet, plagioclase, pyroxenes, amphibole, rutile and ilmenite are represented by white dashed line. Isomodes of garnet, plagioclase, pyroxenes, amphibole, and ilmenite are given in Figs S1, S2, S3 of the Supplementary material.

Fig. 11. (a) *P-T* path of the Punta de li Tulchi granulitized eclogites as inferred from *P-T* pseudosections reported in Figs 9, 10. The H_2O isomodes (wt%) calculated for the pseudosection of Fig. 9 show that sample E9 was H_2O-saturated during its prograde evolution (continuous *P-T* path), whereas it was H_2O-undersaturated at peak-P conditions and during most of the following heating and decompression (dashed *P-T* path). Slightly H_2O-saturated conditions (but with $H_2O < 0.1$ wt%) were reached again at peak-*T* conditions, whereas during the following cooling and decompression the system was H_2O-undersaturated, thus suggesting that the growth of the late amphibole + plagioclase assemblage required the introduction of H_2O from outside. (b) Comparison between the *P-T* path obtained from the Punta de li Tulchi granulitized eclogite (*P-T* path 1, recalculated at $aH_2O = 0.5$ for the sake of comparison) with those obtained for the other Sardinian eclogites (Giacomini *et al*., 2005a: retrogressed eclogites from Golfo Aranci, *P-T* path 2; Cruciani *et al*., 2011: Punta Orvili metabasite, *P-T* path 3).

TABLE CAPTIONS

Table 1. Selected microprobe analyses and structural formula of garnet, pyroxenes, plagioclase, amphibole and ilmenite for Grt-Px layer sample E9. Trivalent iron has been calculated according to Droop (1987) for garnet and by charge balance for pyroxenes. Amphibole structural formula has been calculated according to Mogessie *et al*. (2004). Asterisk indicates mineral composition used in CSpace calculation.

Table 2. Bulk compositions used for pseudosection calculations

SUPPLEMENTARY MATERIAL

Table S1. Selected microprobe analyses and structural formula of garnet, pyroxenes, plagioclase, amphibole and ilmenite for Grt-Px layer sample E10. Trivalent iron has been calculated according to Droop (1987) for garnet and by charge balance for pyroxenes. Amphibole structural formula has been calculated according to Mogessie *et al*. (2004).

Table S2. Selected microprobe analyses and structural formula of plagioclase, amphibole and ilmenite for Am-Pl layer sample E19. Amphibole structural formula has been calculated according to Mogessie *et al*. (2004).

Fig. S1. Isomodes of plagioclase (a), orthopyroxene (b), garnet (c), and clinopyroxene (d) for the *P-T* pseudosection of Fig. 10a.

Fig. S2. Isomodes of plagioclase (a), ilmenite (b), garnet (c), and clinopyroxene (d) for the *P-T* pseudosection of Fig. 10b.
Fig. S3. Isomodes of plagioclase (a), amphibole (b), and garnet (c) for the *P-T* pseudosection of Fig. 10c.

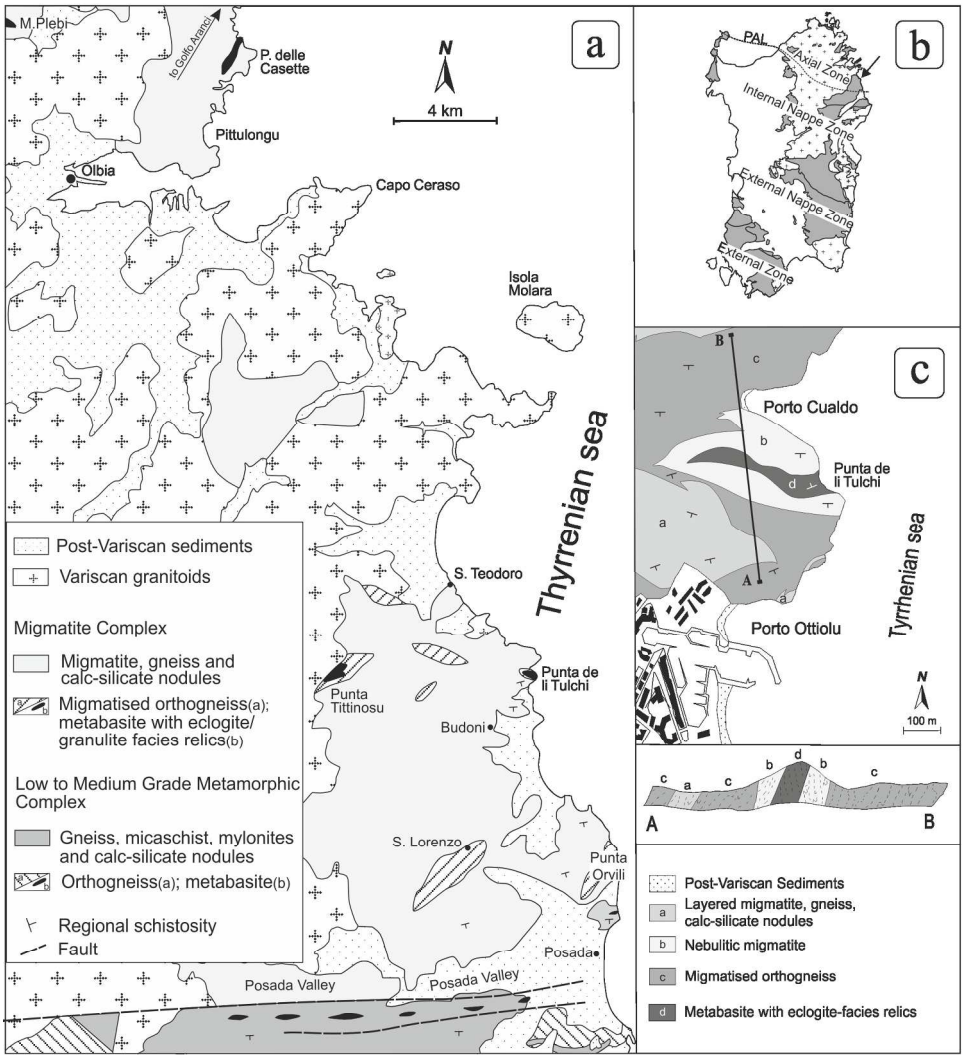

Figure 1
197x207mm (300 x 300 DPI)

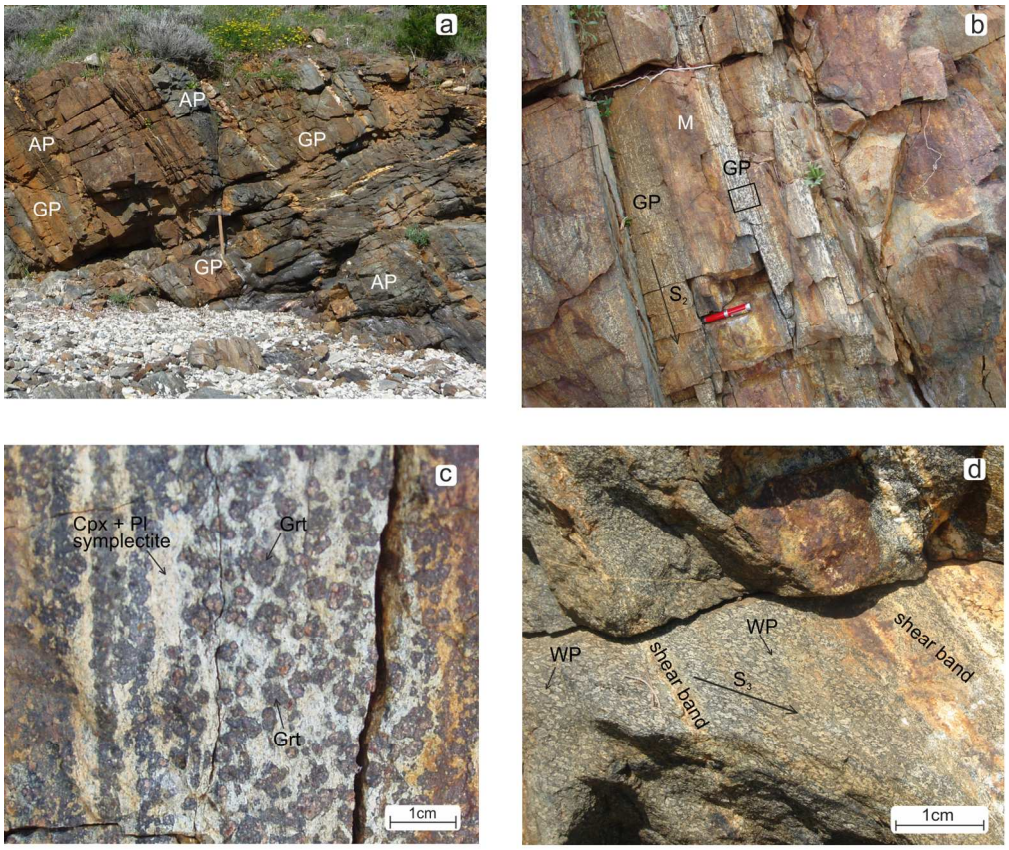

Figure 2
144x122mm (300 x 300 DPI)

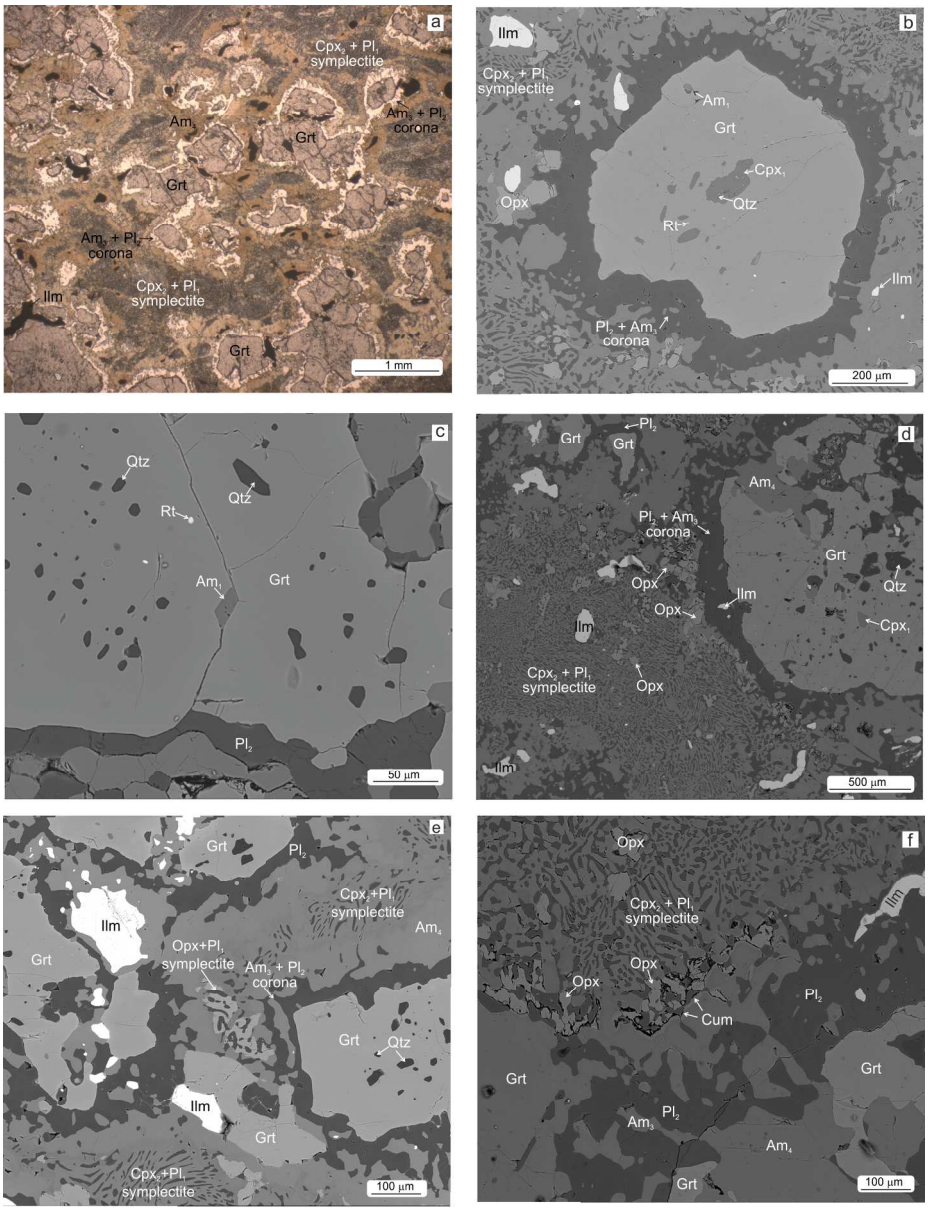

Figure 3
178x232mm (300 x 300 DPI)

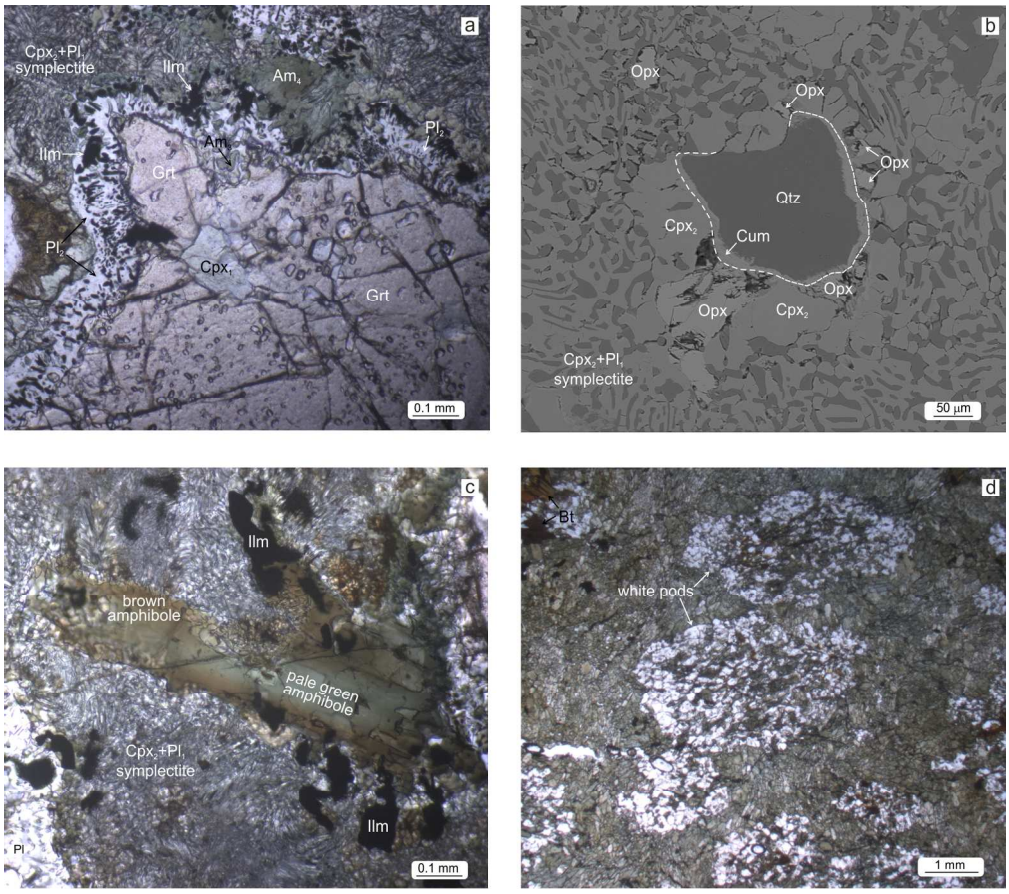

Figure 4
177x156mm (300 x 300 DPI)

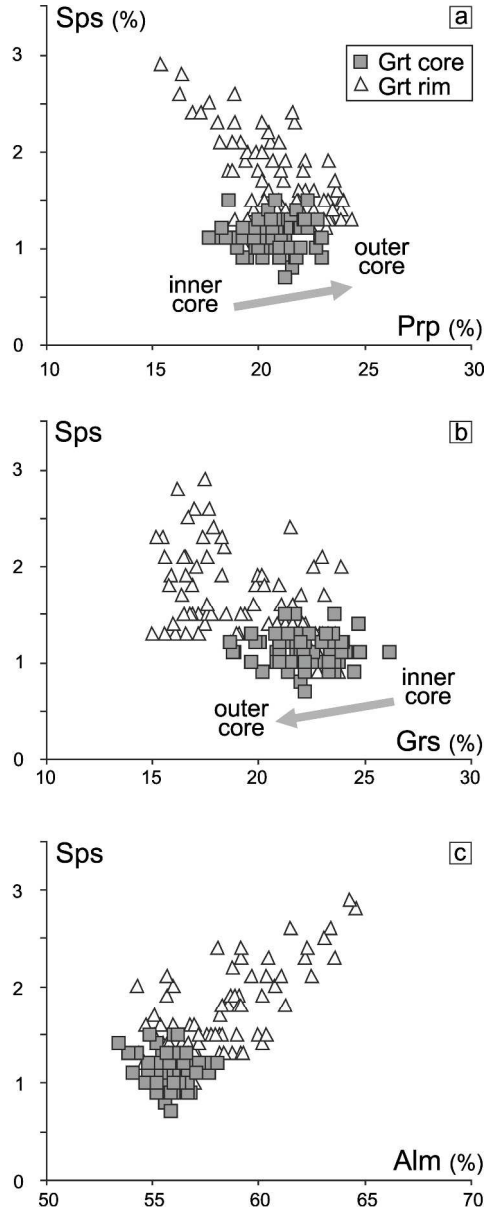

Figure 5
212x542mm (600 x 600 DPI)

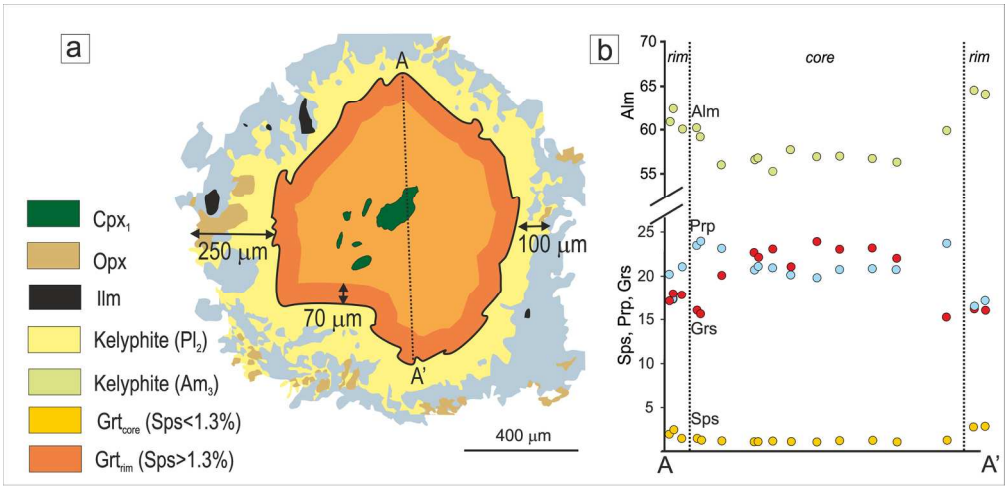

Figure 6
175x84mm (300 x 300 DPI)

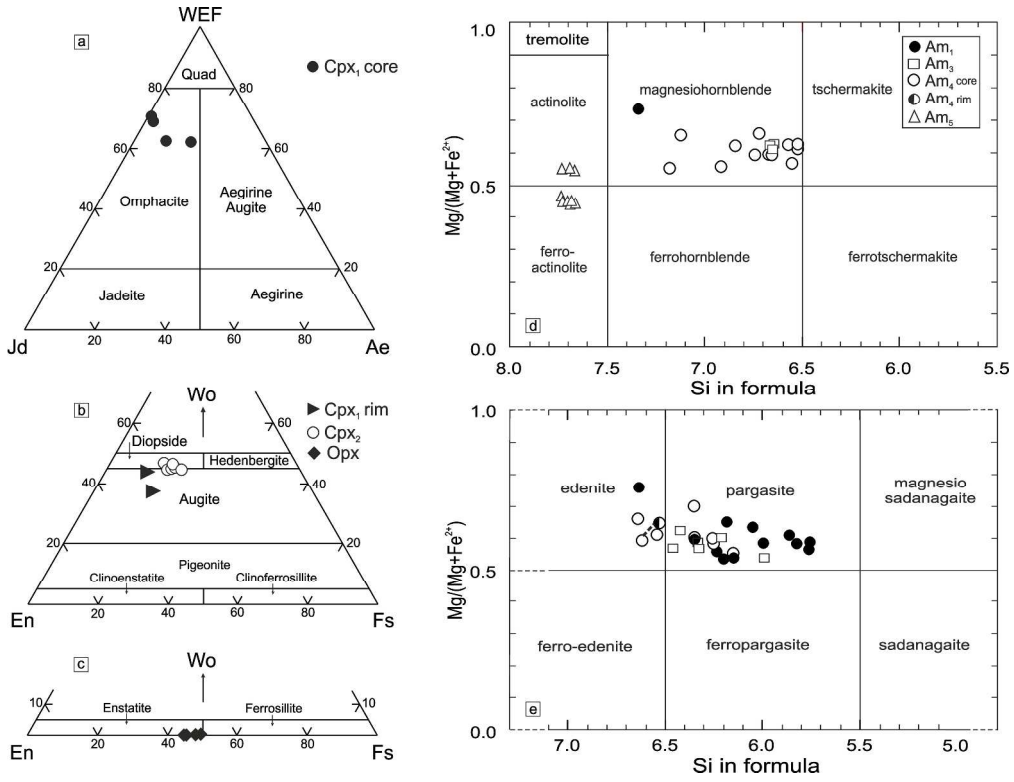

Figure 7
306x234mm (300 x 300 DPI)

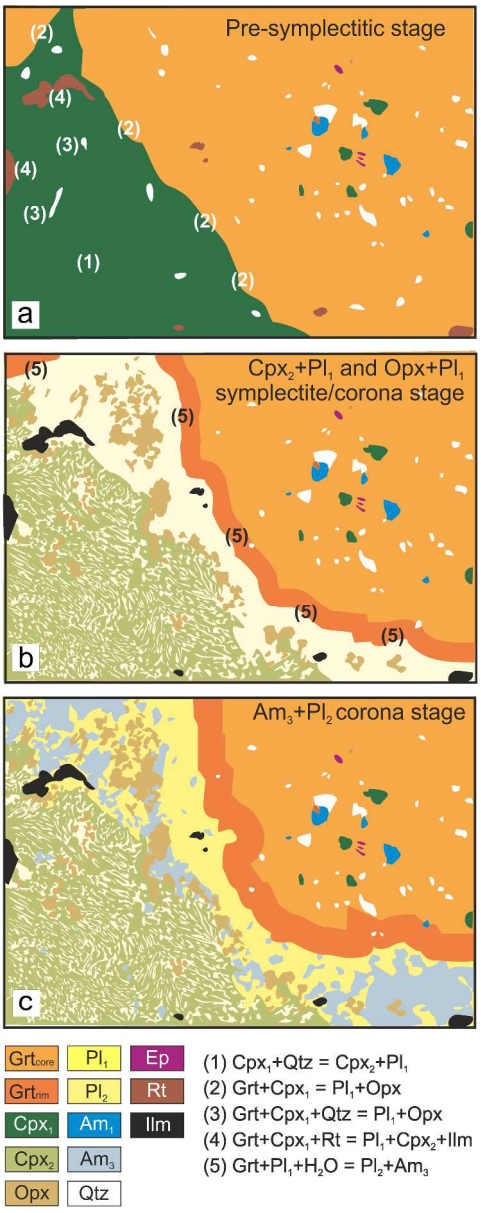

209x526mm (300 x 300 DPI)

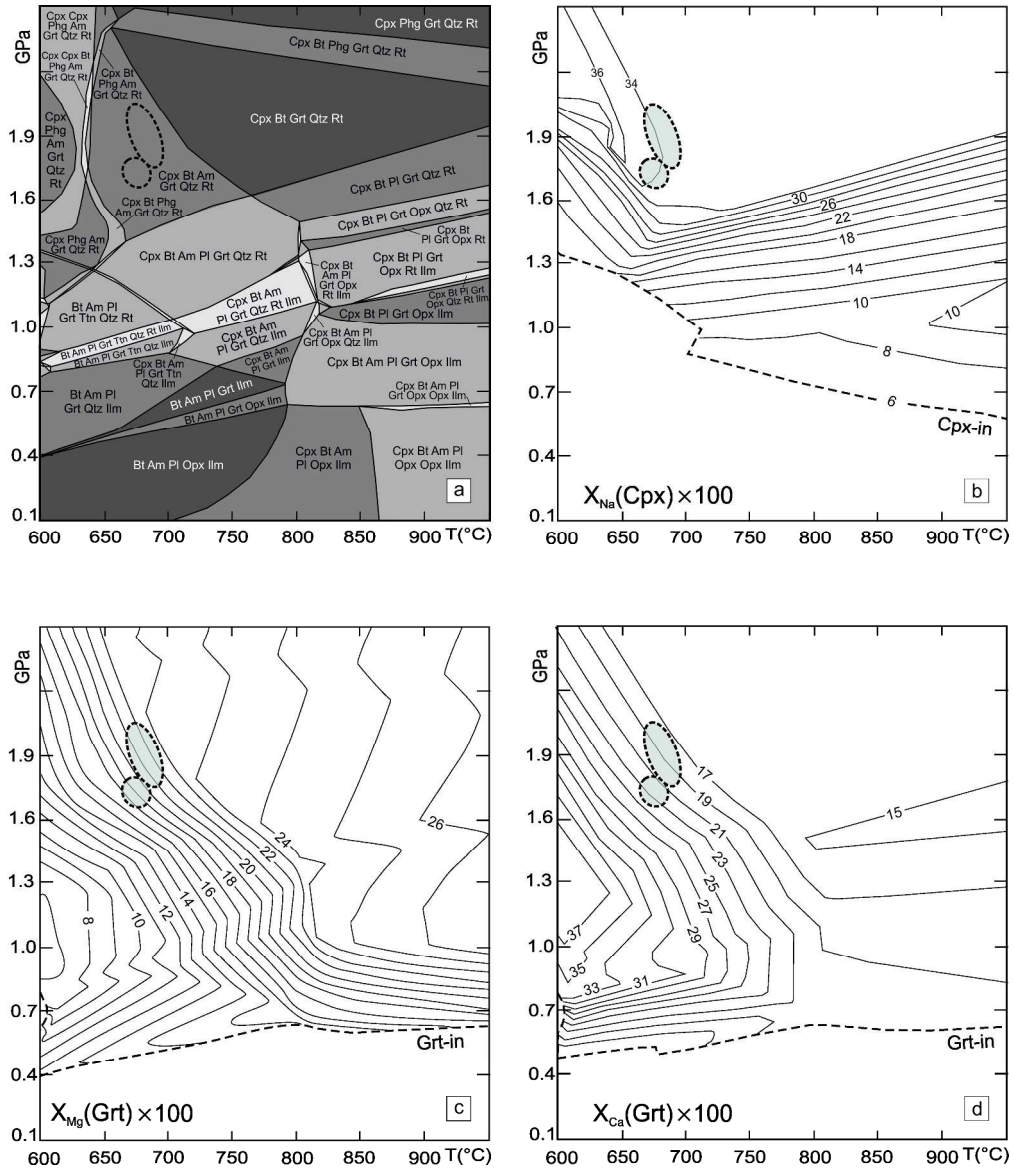

Figure 9
296x343mm (300 x 300 DPI)

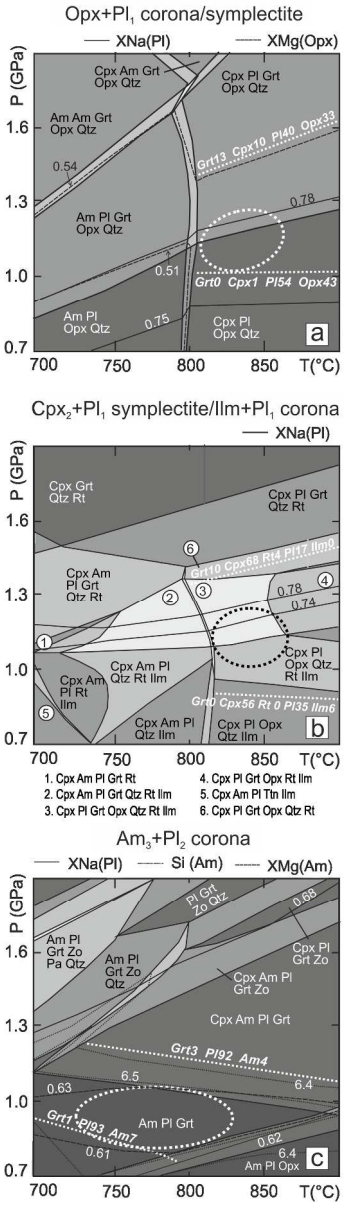

Figure 10
89x304mm (300 x 300 DPI)

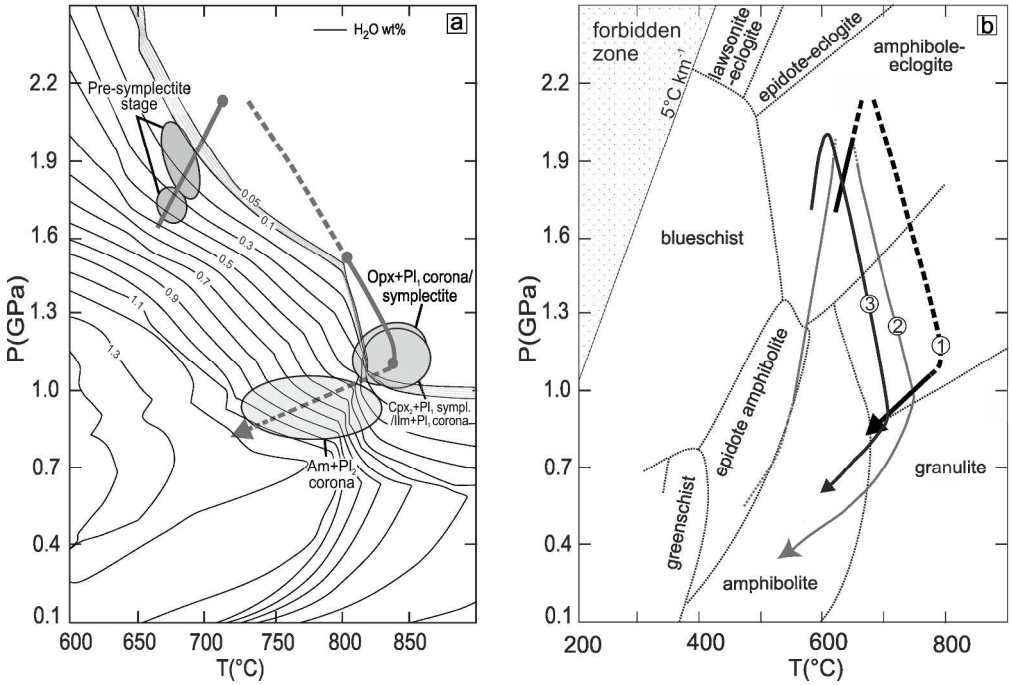

Figure 11
247x185mm (300 x 300 DPI)

Table 1

	Grt core	*Grt out. core	Grt rim	*Cpx_1	*Cpx_2	*Opx	*Pl_1	Pl_1	Pl_2	*Pl_2	Am_1	*Am_3	Am_4	Am_5	Ilm
SiO_2	38.56	38.98	37.97	54.57	51.58	48.84	60.71	62.02	58.00	59.44	40.09	44.63	41.95	51.63	0.02
TiO_2	-	-	-	0.15	0.11	0.08	0.02	-	0.01	0.01	1.16	1.16	1.63	-	52.59
Al_2O_3	21.15	21.25	20.91	7.31	0.97	0.44	23.99	23.59	26.35	25.50	14.74	10.00	13.00	2.05	-
Cr_2O_3	-	-	-		0.06	-	0.01	-	0.02	0.02	-	0.03	0.08	-	-
FeO	26.01	25.99	29.70	8.51	11.22	32.09	0.31	0.28	0.28	0.32	16.87	15.85	15.82	19.64	46.56
MnO	0.52	0.42	1.27	0.10	0.21	0.55	-	-	-	-	-	0.10	0.09	0.11	1.68
MgO	5.44	6.00	4.24	10.05	12.21	16.29	-	-	-	-	10.13	11.67	10.58	11.94	0.10
CaO	8.27	7.35	5.81	15.06	22.21	0.58	5.42	4.63	7.80	6.62	11.06	10.84	11.28	11.44	0.04
Na_2O	-	-	-	4.29	0.39	0.01	8.46	9.02	7.12	7.73	2.70	1.83	2.09	0.15	-
K_2O	-	-	-	-	-	-	0.02	0.06	0.02	0.02	0.24	0.11	0.18	0.10	-
Total	99.95	99.99	99.90	100.04	98.96	98.88	98.94	99.60	99.60	99.66	96.99	96.22	96.70	97.06	100.99
oxy	12	12	12	6	6	6	8	8	8	8	23	23	23	23	3
Si	3.01	3.03	3.01	1.99	1.97	1.94	2.73	2.76	2.60	2.66	6.00	6.65	6.27	7.69	0.00
Al	1.94	1.94	1.95	0.31	0.04	0.02	1.27	1.24	1.39	1.34	2.60	1.76	2.29	0.36	-
Ti	-	-	-	0.00	0.00	0.00	0.00	-	0.00	0.00	0.13	0.13	0.18	-	0.99
Cr	-	-	-	-	0.01	-	0.00	-	0.00	0.00	-	0.00	0.01	-	-
Fe^{2+}	1.66	1.69	1.93	0.25	0.30	0.92	-	-	-	-	1.57	1.55	1.60	2.19	0.98
Fe^{3+}	0.04	0.01	0.03	0.01	0.05	0.13	0.01	0.01	0.01	0.01	0.54	0.42	0.38	0.25	-
Mn	0.03	0.03	0.09	0.00	0.01	0.02	-	-	-	-	-	0.01	0.01	0.01	0.04
Mg	0.63	0.69	0.50	0.55	0.70	0.97	-	-	-	-	2.26	2.59	2.36	2.65	0.00
Ca	0.69	0.61	0.49	0.59	0.91	0.02	0.26	0.22	0.38	0.32	1.77	1.73	1.81	1.83	0.00
Na	-	-	-	0.30	0.03	0.00	0.74	0.78	0.62	0.67	0.78	0.53	0.61	0.04	-
K	-	-	-	-	-	-	0.00	0.00	0.00	0.00	0.05	0.02	0.03	0.02	-
Sum	8.00	8.00	8.00	4.00	4.02	4.02	5.00	5.01	5.00	5.00	15.71	15.40	15.53	15.04	2.01
X_{Na}				0.34	0.03		0.74	0.78	0.62	0.68					
Pyr	0.21	0.23	0.17												
Alm	0.55	0.56	0.64												
Sps	0.01	0.01	0.03												
Grs	0.23	0.20	0.16												
X_{Mg}	0.28	0.29	0.21	0.69	0.70	0.51					0.59	0.63	0.60	0.55	

Table 2

Method	XRF	balanced reaction (2)	balanced reaction (4)	balanced reaction (5)
Micro-domain	whole rock	Opx+Pl_1 sympl./ corona	Ilm+Pl_1 corona and Cpx_2+Pl_1 sympl.	Pl_2+Am_3 corona
Figure	Fig. 9	Fig. 10a	Fig. 10b	Fig. 10c
SiO_2 (wt%)	45.42	56.61	51.18	57.47
TiO_2	2.76	0.00	4.71	0.00
Al_2O_3	13.76	11.83	8.25	25.19
FeO	16.09	15.45	9.95	1.34
MgO	6.85	9.14	7.55	1.00
CaO	10.36	2.87	15.38	8.24
Na_2O	2.05	4.10	2.98	6.76
K_2O	0.11	0.00	0.00	0.00